

## Article

# Crop Mapping and Spatio–Temporal Analysis in Valley Areas Using Object-Oriented Machine Learning Methods Combined with Feature Optimization

Xiaoli Fu <sup>1,2,3</sup>, Wenzuo Zhou <sup>1,2,3,\*</sup>, Xinyao Zhou <sup>1,2,3</sup> and Yichen Hu <sup>1,2,3</sup>

- <sup>1</sup> School of Geographical Sciences, Southwest University, Chongqing 400715, China; fuxiaoli2021@email.swu.edu.cn (X.F.); zxy980206@email.swu.edu.cn (X.Z.); hyc1702@email.swu.edu.cn (Y.H.)
- <sup>2</sup> Chongqing Jinpo Mountain Karst Ecosystem National Observation and Research Station, School of Geographical Sciences, Southwest University, Chongqing 400715, China
- <sup>3</sup> Chongqing Engineering Research Center for Remote Sensing Big Data Application, School of Geographical Sciences, Southwest University, Chongqing 400715, China
- \* Correspondence: zhouwz@swu.edu.cn

**Abstract:** Timely and accurate acquisition of crop planting areas and spatial distribution are deemed essential for grasping food configurations and guiding agricultural production. Despite the increasing research on crop mapping and changes with the development of remote sensing technology, most studies have focused on large-scale regions, with limited research being conducted in fragmented and ecologically vulnerable valley areas. To this end, this study utilized Landsat ETM+/OLI images as the data source to extract additional features, including vegetation index, terrain, and texture. We employed the Random Forest Recursive Feature Elimination (RF\_RFE) algorithm for feature selection and evaluated the effectiveness of three machine learning algorithms—Support Vector Machine (SVM), Random Forest (RF), and Rotation Forest (ROF)—for crop extraction. Then, based on the optimal classifiers, the main crops in the Huangshui basin for the years of 2002, 2014, and 2022 were extracted. Finally, the transfer matrix, the gravity center model, and the Standard Deviation Ellipse (SDE) model were used to analyze the spatio–temporal changes of crops over the past 20 years in the Huangshui basin. The results showed that the spectral, vegetation index, and terrain features played a crucial role in crop extraction. Comparing the performance of the classifiers, the ROF algorithm displayed superior effectiveness in crop identification. The overall accuracy of crop extraction was above 86.97%, and the kappa coefficient was above 0.824. Notably, between 2002 and 2022, significant shifts in crop distribution within the Huangshui basin were observed. The highland barley experienced a net increase in planting area at a rate of 8.34 km<sup>2</sup>/year, while the spring wheat and oilseed rape demonstrated net decreases at rates of 16.02 km<sup>2</sup>/year and 14.28 km<sup>2</sup>/year, respectively. Furthermore, the study revealed that highland barley exhibited the most substantial movement, primarily expanding towards the southeast direction.

**Keywords:** crop mapping; machine learning; object-oriented; feature selection; Huangshui basin



**Citation:** Fu, X.; Zhou, W.; Zhou, X.; Hu, Y. Crop Mapping and Spatio–Temporal Analysis in Valley Areas Using Object-Oriented Machine Learning Methods Combined with Feature Optimization. *Agronomy* **2023**, *13*, 2467. <https://doi.org/10.3390/agronomy13102467>

Academic Editors: Dan Li, Yingying Dong and Qiong Zheng

Received: 23 August 2023

Revised: 19 September 2023

Accepted: 22 September 2023

Published: 24 September 2023



**Copyright:** © 2023 by the authors. Licensee MDPI, Basel, Switzerland. This article is an open access article distributed under the terms and conditions of the Creative Commons Attribution (CC BY) license (<https://creativecommons.org/licenses/by/4.0/>).

## 1. Introduction

Food security has been a long-standing, complex, and highly concerning issue in China [1]. In the context of global climate change, the need for dynamic, wide-scale, fast, and timely spatial information on crops is becoming increasingly urgent [2,3]. Accurate information on the spatio–temporal changes of crops is crucial for government departments when formulating food policies, promoting agricultural development, and ensuring food and ecological security [4,5].

The traditional methods used in China to collect information on crops primarily involve analyzing statistical data based on administrative divisions such as districts, counties, cities, and provinces. While this approach helps one to grasp the overall situation of crop

areas for different administrative levels, it lacks spatial details and suffers from temporal delays [6]. The use of remote sensing to monitor crops and support their management has received increasing attention in recent years with the launch of sensor satellites carrying different resolutions [7]. Compared with traditional statistical methods, crop distribution extraction using remote sensing means is more accurate, effective, and less costly.

At present, crop identification using multispectral data from the MODIS, Landsat, SPOT, Sentinel, and other sources has shown promising results [6,8–10]. However, accurate crop-type mapping remains challenging due to spectral similarity, crop diversity, and intra-class variability caused by environmental conditions [11]. To develop accurate crop spatial distribution maps, researchers have utilized spectral, vegetation index, texture, and other features for crop identification. However, including all the features in the classification process can weaken classifier performance, leading to the issues of information redundancy. In recent years, feature selection methods have been applied to crop classification with varying degrees of success. The Random Forest Recursive Feature Elimination (RF\_RFE), which can quantify the relative importance of each variable, is commonly used for high-dimensional feature selection [12,13].

The crop classification methods with more applications and more mature technologies are mainly pixel-based and object-oriented classification [14]. Pixel-based crop classification struggles to maintain the integrity of objects [15], often resulting in the “salt-and-pepper” phenomenon during the classification process. This phenomenon may result in the misclassification of certain areas or objects within the image, ultimately reducing the accuracy and reliability of crop classification. Object-based classification is developed to fully exploit the information contained in high-resolution imagery. This method can utilize spatial, textural, and contextual features of image-objects [16]. Some researchers have demonstrated the advantages and potential of object-based classification even in medium-resolution remote sensing imagery [17]. Furthermore, many scholars have successfully applied this technique to crop classification, yielding satisfactory results [18–20].

With the support of abundant satellite imagery resources, numerous classification techniques have been developed to extract the spatial distribution of crop planting. These techniques can be broadly categorized into the following: automatic extraction, based on phenological information; traditional supervised and unsupervised classification methods; and the emerging machine learning methods in recent years [11]. Extracting crop planting structures based on phenological information does not require the acquisition of supervised information, and is simple to operate and suitable for automatic extraction of crop planting structures in a wide area [21]. However, in this method, it is difficult to distinguish the planting structure of crops with similar phenological information [22]. Conventional supervised and unsupervised classification methods have gradually become inadequate for extracting crops in complex regions. In recent years, with further research advancements, machine learning classification algorithms such as the K-nearest Neighbors (KNN), Decision Tree (DT), Support Vector Machine (SVM), and Random Forest (RF) have been developed [23]. Among these commonly used machine learning algorithms, the SVM and RF have been widely applied in crop-type mapping due to their efficient, accurate, and robust identification capabilities [24–26]. The SVM is considered to be one of the most classical machine learning algorithms, and its essence is a maximum interval classification method [27]. The RF is an integrated-learning method based on decision trees that is becoming increasingly common in remote sensing applications due to its flexible nonparametric nature and ability to limit overfitting [28,29].

However, different classifiers exhibit varying sensitivities to different data sources and spectral characteristics of crops, and there is currently no universal classifier. The Rotation Forest (ROF) algorithm, initially proposed by Rodriguez et al. [30] in 2006, is an enhancement of the RF algorithm. The algorithm’s core is rotating the feature axes of initial data using the Principal Component Analysis (PCA). This rotation provides diverse training samples to the base classifier, enhancing its variability and leading to improved classification accuracy [31,32]. Researchers have applied the ROF algorithm to vegetation

classification and achieved better results than with the RF algorithm [33]. The potential of this algorithm in crop mapping still requires further development and exploration.

Currently, crop research is primarily focused on large-scale regions such as global or national levels, while research on specific areas with complex terrain is relatively limited. Furthermore, the research has mainly concentrated on major crops such as rice, wheat, and rapeseed, with less attention given to region-specific crops like highland barley. Therefore, there is a need for more in-depth research in these specific regions to optimize crop-mapping approaches. Such research will contribute to a better understanding and addressing of the challenges in crop cultivation and management in specific regions [34].

Specialized small-scale agriculture mapping encounters challenges related to data sources and mapping methods, further compounded by the distinct geographic environment of specific regions. Despite the emergence of promising mapping techniques, the adaptability of crop classification and mapping methods in such regions remains an area warranting extensive exploration. Additionally, there is a relative shortage of research on the extraction and monitoring of specific crops over multiple time periods in particular regions. Conducting multi-temporal crop extraction and spatial evolution analyses can provide valuable insights for agricultural decision-makers, aiding their understanding of food production, crop diversity, and supply–demand dynamics.

In view of these considerations, our study centers on the Huangshui basin, employing the Landsat ETM+/OLI imagery available during the study period as our foundational dataset. We preprocess the imagery using data fusion and vegetation-enhancement techniques to elevate its spatial resolution, meeting the requisites for crop mapping in small-scale regions. To capitalize on relevant geographic environmental features, auxiliary factors such as terrain and texture are integrated into the feature selection process for crop classification. The primary objectives encompass the following: (1) assessing the significance of various features in crop classification through feature selection algorithms; and (2) evaluating the suitability of object-oriented machine learning algorithms for crop extraction in intricate terrain settings. Moreover, the study strives to achieve the following: (3) accomplish crop mapping for the Huangshui basin in the years 2002, 2014, and 2022; and (4) investigate spatio—temporal variations in crop planting structures within the region over the past two decades.

## 2. Materials and Methods

### 2.1. Study Region

The Huangshui basin, situated approximately between 36°04' N to 37°43' N and 100°68' E to 103°26' E, lies on the border between the Qinghai province and the Gansu province (Figure 1), in China. It exhibits a diverse topography characterized by substantial elevation changes, steep slopes, and an intricate network of rivers crisscrossing the landscape [35]. The topography of the basin is higher in the northwest and lower in the southeast, with an altitude of 1542–4800 m. Due to the influence of the climatic and topographic factors associated with the Qinghai–Tibet Plateau, the area features an uneven precipitation distribution and variations in the local temperature. The average annual temperature within the basin is about 6.4 °C. Precipitation is mainly concentrated in the summer, with an average annual precipitation of about 306 mm. It has an arid and semi-arid continental climate [36]. The Huangshui basin is a crucial river-valley agricultural region in the Qinghai province, with 317,000 hm<sup>2</sup> of arable land, accounting for 52.3% of the total arable land area in the province. The effective irrigation area is about 120,000 hm<sup>2</sup>, accounting for 48% of the effective irrigation area in the province [37]. The planting types of crops in the basin are relatively stable, mainly including highland barley, spring wheat, and oilseed rape, etc. Due to the temperature conditions, the agricultural production in the Huangshui basin follows an annual single-cropping system, concentrated in the river-valley area [38].

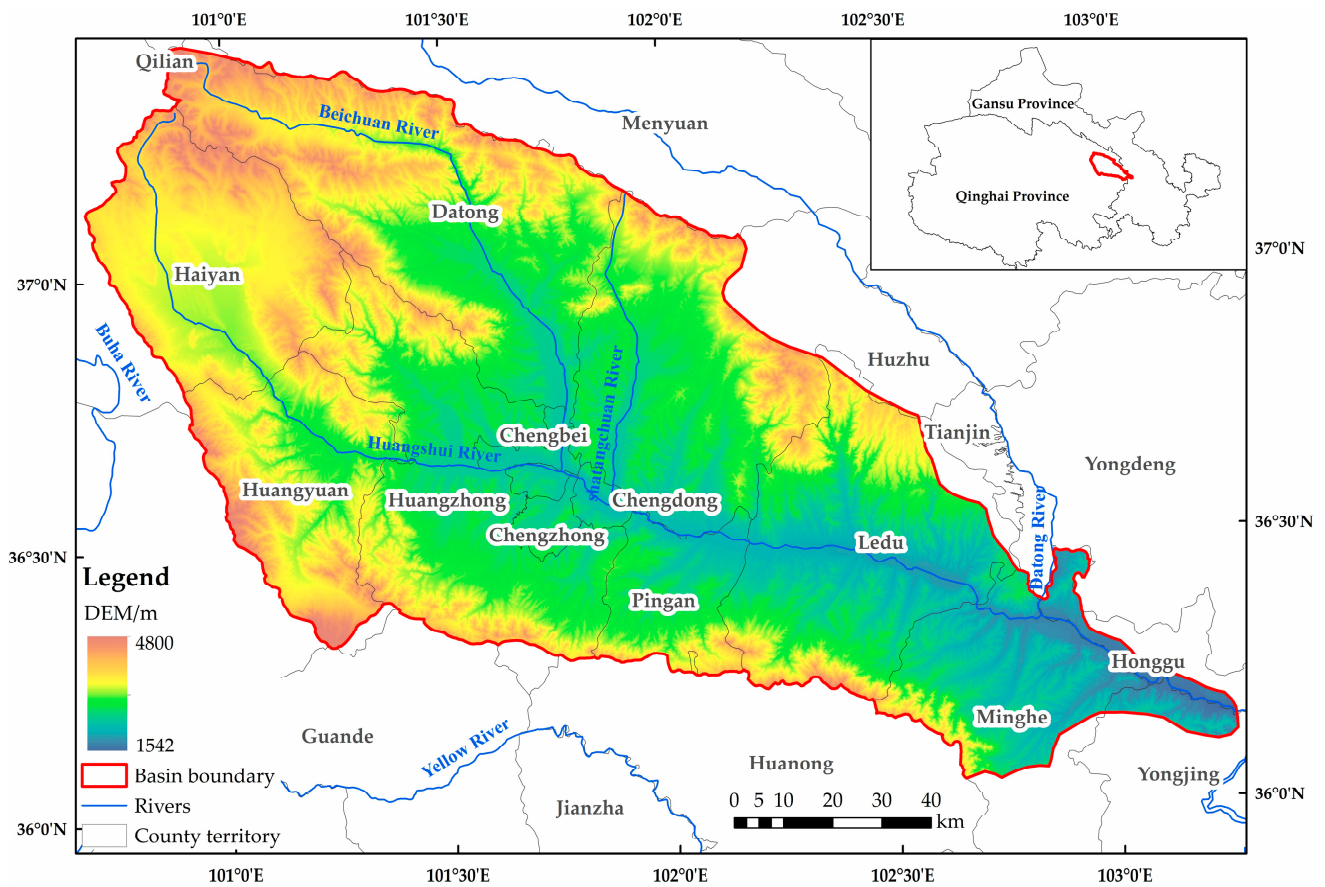


**Figure 1.** The study area (including digital elevation information, county-level administrative districts, and rivers in the basin).

## 2.2. Data Source and Preprocessing

This study mainly extracted three main crop types—highland barley, spring wheat, and oilseed rape—in the Huangshui basin based on the cropland data. The land-use data were obtained from the China Land Cover Dataset (CLCD) generated by Yang et al. [39] using the RF algorithm based on Landsat data.

The multispectral data were obtained from the Google Earth Engine (GEE) platform after processing steps including cloud removal, mosaic, and clip. The Landsat 7 ETM + data in July 2002 and the Landsat 8 OLI data in July 2014 and 2022 were selected. The multispectral data consist of red, green, blue, near-infrared (NIR), and two short-wave infrared (SWIR) bands, with a spatial resolution of 30 m. Additionally, the data include a panchromatic band with a higher resolution of 15 m.

To enhance the spatial resolution of the data, we applied the Gram-Schmidt Pan Sharpening (GS) fusion algorithm within the ENVI 5.6 software to merge the Landsat's high-resolution panchromatic channel image with its low-resolution multispectral channel image. This fusion process enhanced the overall spatial resolution to 15 m. Furthermore, we conducted vegetation-enhancement processing on the images using the Vegetation Enhance plugin, which is an ENVI extension tool. This processing was designed to emphasize the distinctions among various crop types, as illustrated in Figure 2. In addition to the original spectral bands, the Normalized Vegetation Index (NDVI), texture features, and terrain features were incorporated for crop classification.

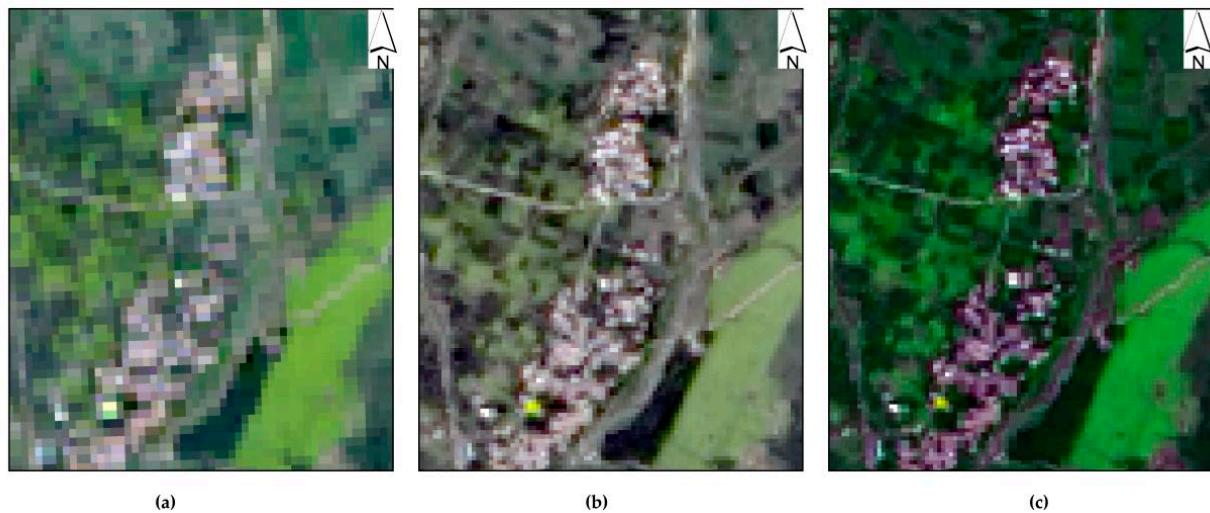


**Figure 2.** Comparison of local images before image processing: (a) Landsat 8 true-color composite display with 30 m resolution; (b) true-color display after data fusion with 15 m resolution; and (c) true-color display after vegetation enhancement based on (b).

The Digital Elevation Model (DEM) data, obtained from the United States' National Aeronautics and Space Administration (NASA), had a spatial resolution of 12.5 m. Based on the DEM data, slope and aspect data were derived and resampled to a resolution of 15 m.

The statistics on crop planting areas were sourced from the National Tibetan Plateau Data Center website (<https://data.tpdc.ac.cn> accessed on 1 May 2023) and the Qinghai Statistical Yearbook, serving as auxiliary validation for crop classification.

The sample data referenced the distribution data of oilseed rape in China from 2017 to 2022 [40], wheat distribution data in China from 2001 to 2015 [41], and historical imagery from Google Earth. For the years 2002, 2014, and 2022, a total of 2639, 2511, and 2251 samples were selected, respectively.

### 2.3. Methods

#### 2.3.1. Multi-Scale Segmentation

Object-oriented classification is an intelligent, automated image-analysis method, which differs significantly from traditional classification methods in that it operates at the scale of image-objects rather than individual pixels. In the real world, objects refer to geographic entities or phenomena, while in object-oriented classification, objects are defined as image patches resulting from image segmentation, referred to as image-objects or object units [18]. In this study, the multi-scale segmentation method within the eCognition 9.4 software was employed to partition the images into parcel objects. Notably, the accuracy of crop mapping can be significantly influenced by the choice of segmentation parameters [42]. We employed the automatic segmentation scale parameter selection ESP2 tool that identified the best segmentation scale to be 47. By referring to related articles [43] and comparing the segmentation effect with different parameters at 0.1 step, the best segmentation effect was achieved when the shape was set to 0.1 and the compactness was set to 0.5.

#### 2.3.2. Feature Optimization

The RF\_RFE is a hybrid feature-selection approach of an embedded and a wrapper, and the algorithm process is as follows [28,44]. To begin, the RF model was trained using training data, and the importance of each feature was determined based on its classification contribution. Next, the features with the lowest importance were removed based on the ranking, and the RF model was retrained using the updated set of features. This iterative process continued until the feature set became empty. Finally, the list of the performance

measures generated for each subset after running the model was used to filter and identify the optimal feature subset.

### 2.3.3. Machine Learning Classification Methods

#### (1) SVM

The SVM is a powerful supervised learning algorithm, introduced by Cortes and Vapnik [45] in 1995. The goal of SVM is to find an optimal hyperplane (a line in a two-dimensional space or a hyperplane in a multidimensional space) that separates data points of different classes. The SVM is capable of effectively handling nonlinear problems; this is achieved through the use of kernel techniques [46]. The Kernel techniques allow data to be mapped from the original space to a higher dimensional space where the data can be linearly separated. The choice of kernel function significantly impacts the accuracy of the SVM model, with commonly used kernel functions including the linear kernel, polynomial kernel, and Radial Basis Function (RBF) kernel, among others.

In practical scenarios, data may not be linearly separable, leading to the introduction of a soft margin. A soft margin allows for some data points to not strictly meet the margin requirements, but introduces a penalty parameter (usually denoted as  $C$ ) to balance the margin size and the penalty for misclassification. The choice of  $C$  influences the model's generalization ability.

When the SVM algorithm was applied to classify data in this study, the following choices were made: the RBF was selected as the kernel function; the kernel function parameter Gamma was set to 1; the penalty factor  $C$  was set to 10; and other parameters were set to default.

#### (2) RF

The RF is an ensemble learning method proposed by Breiman [29] in 2001. It combines multiple decision tree models for classification. These decision trees are constructed by randomly sampling different subsets (with replacement) from the training data and by selecting features randomly. Each decision tree serves as a basic classifier and splits data based on their features to minimize errors. Each tree produces a prediction, and the final prediction is determined by a majority vote [47].

The RF algorithm introduces the concept of randomness, making each decision tree unique. The randomness involves the random selection of samples from the training data and random feature selection from the feature set. This helps reduce overfitting and enhances the model's generalization ability. The key parameters in RF include the number of decision trees, the randomness in feature selection, tree depth, and more. Typically, the best parameter configuration is chosen through cross-validation.

When the RF algorithm was applied to classify data in this study, the number of base classifiers was set to 140. The number of features to be considered for finding the best segmentation was set to four. The minimum number of samples needed at the leaf nodes was set to two, and other parameters were set to default values.

#### (3) ROF

The ROF algorithm is an extension and improvement of the RF [30]. The algorithm enhances classification performance by rotating original features into new ones. This rotation process is based on the PCA, which attempts to identify the main directions of variance in the data and map the data onto these primary directions. The ROF introduces diversity by constructing decision trees in different feature spaces. Each decision tree is built in a feature space that has been rotated, resulting in different feature combinations for each tree. This helps reduce model variance and improve generalization performance. Similar to the RF, the ROF algorithm uses a voting mechanism for classification. Each decision tree classifies samples, and the final classification result is determined by the votes of multiple trees [48]. The key parameters in the ROF include the number of base classifiers (decision trees) and the subset size for feature rotation partitions.

When the ROF algorithm was applied to classify data in this study, the number of base classifiers  $L$  was set to 290, and the number of divided feature subsets  $K$  was set to 4.

This paper, based on the Python programming language, explores the effectiveness of the above three machine learning algorithms in crop classification.

#### 2.3.4. Accuracy Verification

For the crop classification results, the User Accuracy (UA), Producer Accuracy (PA), Average Accuracy (AA), Overall Accuracy (OA), and kappa coefficients were used for an evaluation based on the confusion matrix. The crop areas extracted in this paper were also compared with the data published in the Statistical Yearbook to judge the accuracy of the extracted results.

#### 2.3.5. Gravity Center Model

The gravity center, which originates from the field of physics, is the point where gravity is uniformly applied to each part of an object [49]. The gravity center of crop spatial distribution is the point at which the crop acreage reaches equilibrium in all directions within a certain geographic area. The migration direction of gravity center indicates the change in direction of crop planting, and the migration length indicates the degree of crop change in space [50]. The formula for calculating the gravity center of crop spatial distribution is as follows:

$$X_j = \frac{\sum_{i=1}^n A_{ij}x_i}{\sum_{i=1}^n A_{ij}}; Y_j = \frac{\sum_{i=1}^n A_{ij}y_i}{\sum_{i=1}^n A_{ij}} \quad (1)$$

In the equation,  $X_j$  and  $Y_j$  represent the gravity centroid geographical coordinates of a certain crop in the  $j$ -th year within the study area.  $x_i$  and  $y_i$  represent the gravity centroid geographical coordinates of the crop in the  $i$ th plot.  $A_{ij}$  represents the planting area of the crop in the  $i$ -th region in the  $j$ -th year.

$$D_m = \sqrt{(X_{k+m} - X_k)^2 + (Y_{k+m} - Y_k)^2} \quad (2)$$

$D_m$  represents the gravity centroid movement distance of the planting area over an interval of  $m$  years.  $(X_{k+m}, Y_{k+m})$  and  $(X_k, Y_k)$  represent the gravity centroid coordinates of the planting area in the  $(k+m)$ -th year and the  $k$ -th year, respectively.

#### 2.3.6. Standard Deviation Ellipse Analysis

The Standard Deviation Ellipse (SDE) model is a specific presentation of spatial distribution characteristics through ellipses, which can reveal the spatial distribution of geographic elements from several perspectives [51,52]. For example, the axis length of ellipse indicates the direction of spatial-element distribution, and the shape of ellipse indicates the dispersion degree of spatial elements. In this paper, the changes of the concentrated distribution area, distribution range, and direction of crops in the Huangshui basin are studied using the SDE model.

### 3. Results

#### 3.1. Comparison of Machine Learning Classification Methods Based on Feature Optimization

Based on the multi-scale segmented objects, nine spectral features, NDVI, three terrain features, and eight texture features were extracted to participate in the classification. The 21 features extracted in 2002, 2014, and 2022 were input into the RF\_RFE algorithm for feature optimization, and the final number of retained features was 17, 15, and 16, respectively. All spectral features, NDVI, and terrain features were retained, and some texture features were filtered out. According to the importance analysis (Figure 3), it can be seen that the NDVI, NIR band, green band, and Max\_diff contributed more to the crop identification process, while the contributions of texture features were relatively small.

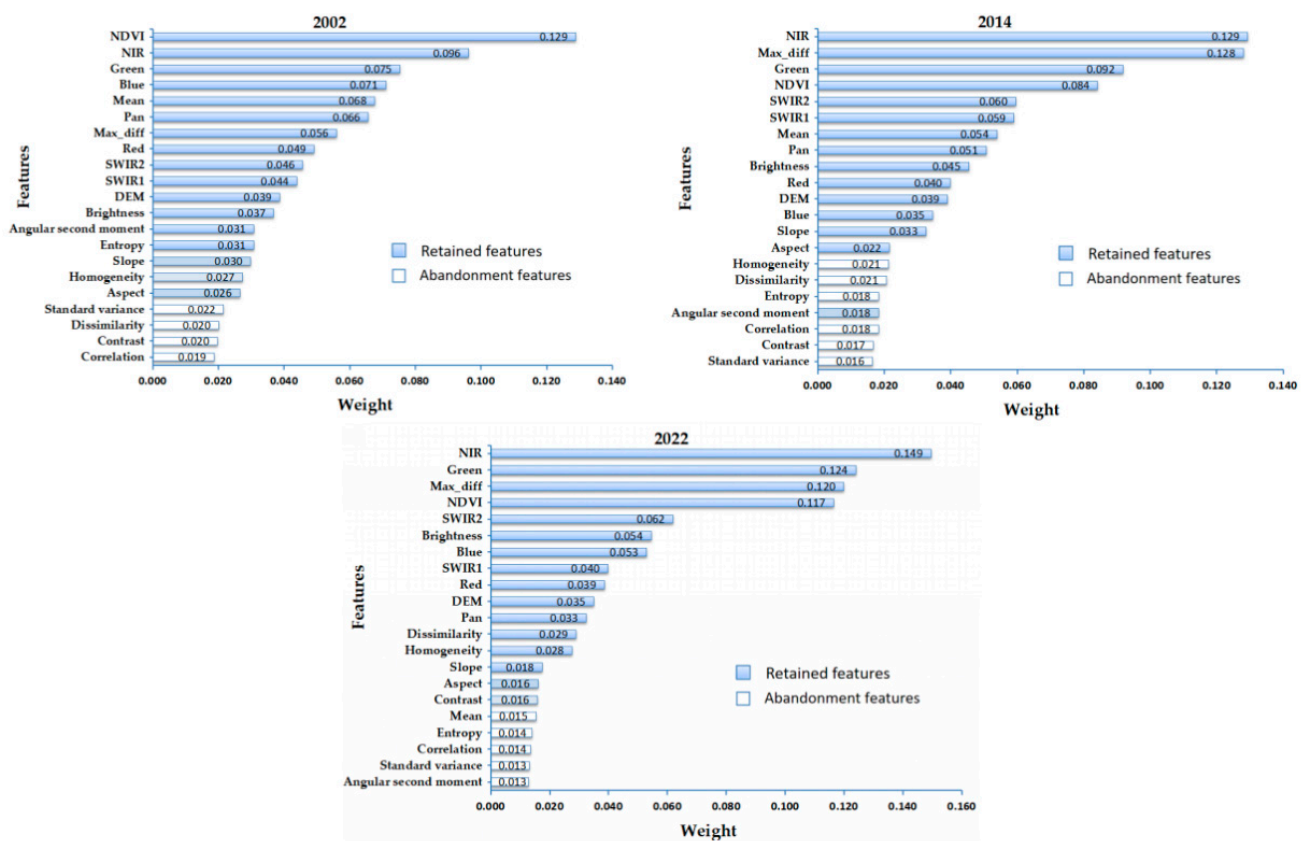


**Figure 3.** Feature importance analysis and selection results of the crop classification in the Huangshui basin.

The data before and after the feature selection were input into different classifiers and run 10 times to obtain the average accuracy, as shown in Figure 4. The crop identification accuracy after the feature selection in 2002, 2014, and 2022 improved by 1.43–2.19%, 0.60–1.41%, and 1.99–2.18%. All three machine learning classification algorithms based on feature selection achieved a good classification performance with a validation accuracy above 83.92%. Among them, the ROF algorithm achieved the best classification performance with validation accuracies of 87.62%, 90.13%, and 91.13% for 2002, 2014, and 2022 crop classification, respectively. The ROF algorithm was subsequently selected to complete the crop classification mapping of the Huangshui basin.

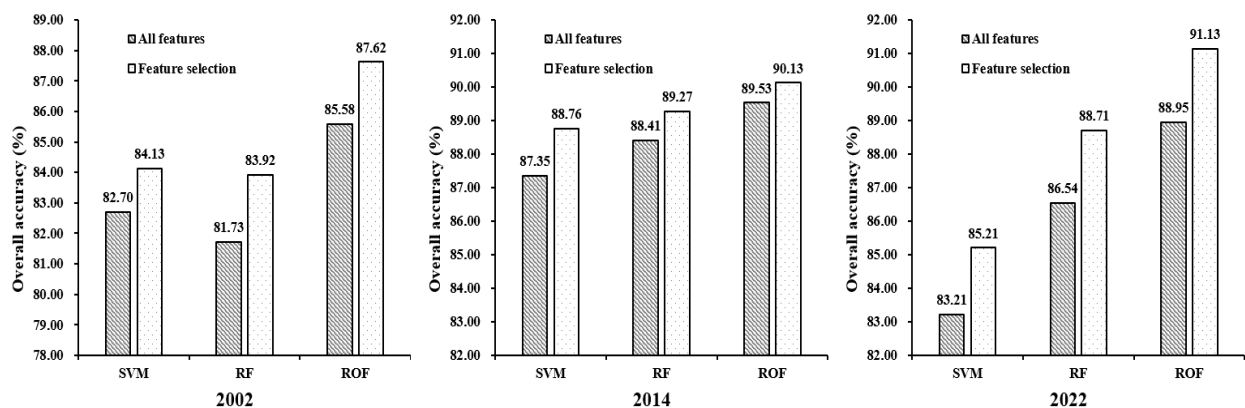


**Figure 4.** Comparison of accuracy of different machine learning algorithms in the crop identification in the Huangshui basin.

### 3.2. Extraction Accuracy and Spatial Distribution of Crop Planting Structure

The spatial distribution of crops in the Huangshui basin in 2002, 2014, and 2022 was extracted using the ROF algorithm. Based on the confusion matrix, the crop extraction accuracy of the Huangshui basin was calculated (Table 1). The OA of crop extraction was above 86.97%; the AA was above 86.51%; the kappa coefficient was above 0.824. Among the main crops, spring wheat had the best identification performance, with a PA ranging from 90.62% to 96.72% and a UA ranging from 87.50% to 88.94%. Next was highland barley, with a PA ranging from 82.09% to 85.71% and a UA ranging from 84.03% to 90.16%. Finally, the PA of oilseed rape ranged from 77.57% to 85.19% and the UA of oilseed rape ranged from 81.77% to 89.44%.

**Table 1.** Accuracy of crop extraction based on the ROF algorithm in the Huangshui basin.

	2002				2014				2022			
	HB	SW	OR	OC	HB	SW	OR	OC	HB	SW	OR	OC
HB *	100	4	13	2	110	3	20	1	102	1	14	2
SW *	11	203	9	1	2	203	10	0	1	177	5	0
OR *	8	12	157	15	10	23	166	15	9	16	161	3
OC *	0	13	8	191	0	0	1	217	6	5	0	125
UA (%)	84.03	87.5	81.77	90.95	90.16	88.65	84.26	93.13	86.44	88.94	89.44	96.15
PA (%)	84.03	90.62	83.96	89.6	82.09	94.42	77.57	99.54	85.71	96.72	85.19	91.91
AA (%)		86.51				88.4				89.88		
OA (%)		86.97				89.12				90.11		
Kappa		0.824				0.853				0.866		

\* HB, SW, OR, and OC in the table are abbreviation for highland barley, spring wheat, oilseed rape, and other crops, respectively.

According to the Statistical Yearbook of the Qinghai province, the total planted area of crops in Xining City and Haidong City, which roughly overlaps with the boundary of the Huangshui basin, was calculated. The extracted crop area data from this study were compared with the data from the Statistical Yearbook (Table 2). The results showed that the average differences in the planted area of highland barley, spring wheat, and oilseed rape were 20.88 km<sup>2</sup>, 123.05 km<sup>2</sup>, and 103.28 km<sup>2</sup>, respectively. The reason for these differences may be that the statistical data region does not align perfectly with the boundary of the Huangshui basin. Overall, the crop extraction area obtained in this study closely matches the statistical data, indicating its suitability for subsequent research.

**Table 2.** Comparison of crop extraction area based on the Statistical Yearbook in the Huangshui basin (unit: km<sup>2</sup>).

	2002		2014		2022	
	ROF	Statistical Yearbook	ROF	Statistical Yearbook	ROF	Statistical Yearbook
Highland Barley	260.19	245.69	294.00	309.77	426.92	459.30
Spring Wheat	1037.63	1169.91	811.74	630.99	717.28	773.40
Oilseed Rape	1078.72	856.09	957.31	895.20	793.07	818.20
Other crops	2297.84	1927.80	1855.86	1842.82	1465.62	1296.50
Total cultivated land	4674.38	4199.49	3918.91	3678.77	3402.89	3347.40

From 2002 to 2022, the main distribution of highland barley, spring wheat, oilseed rape, and other crops in the Huangshui basin was observed in the Datong county, the Huangzhong county, and the Huzhu county (Figure 5). During the period from 2002 to 2022, oilseed rape had the widest spatial distribution among the major crops planted in the Huangshui basin, followed by spring wheat, and, lastly, highland barley.

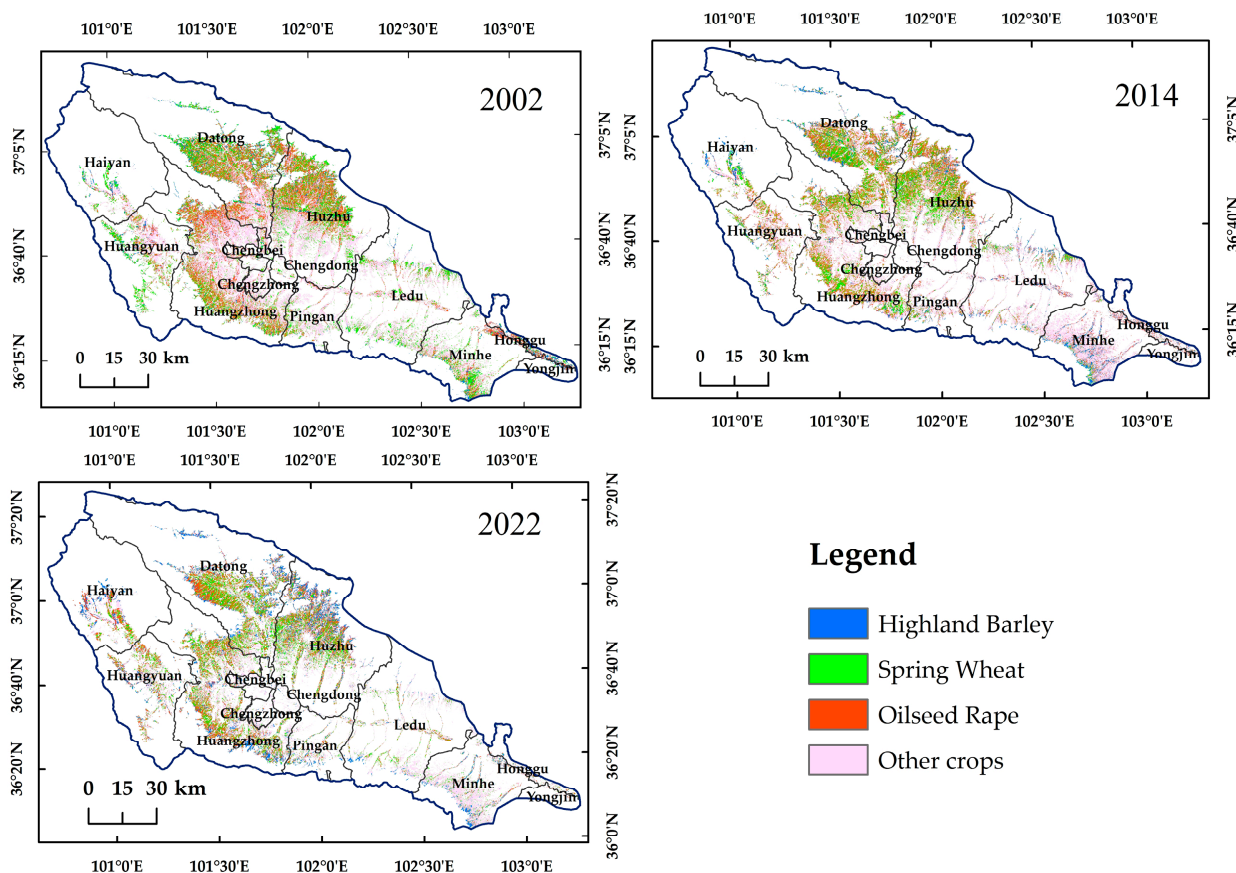


**Figure 5.** The crop classification results in the Huangshui basin based on the ROF algorithm.

The cultivation area of highland barley in the Huangshui basin in 2002, 2014, and 2022 was 260.19 km<sup>2</sup>, 294.00 km<sup>2</sup>, and 426.92 km<sup>2</sup>, respectively, showing an overall increasing trend, with an average growth rate of 8.34 km<sup>2</sup>/year. The cultivation area of spring wheat in the Huangshui basin in 2002, 2014, and 2022 was 1037.63 km<sup>2</sup>, 811.74 km<sup>2</sup>, and 717.28 km<sup>2</sup>, respectively, showing an overall decreasing trend, with an average decline rate of 16.02 km<sup>2</sup>/year. The cultivation area of oilseed rape in the Huangshui basin in 2002, 2014, and 2022 was 1078.72 km<sup>2</sup>, 957.31 km<sup>2</sup>, and 793.07 km<sup>2</sup>, respectively, showing an overall decreasing trend, with a decelerating rate of 14.28 km<sup>2</sup>/year. In the past 20 years, the rate of increase in the highland barley’s cultivation area has been accelerating. The rate of decrease in the spring wheat’s cultivation area has slowed down. The rate of decrease in the oilseed rape’s cultivation area has been increasing. The cultivation areas of other crops and the total arable land area in the Huangshui basin have both showed a decreasing trend.

### 3.3. Evolution Analysis of Crop Planting Structure

The transfer matrix of crops’ areas in the Huangshui basin are shown in Table 3. From 2002 to 2014, the outflow areas of highland barley, spring wheat, and oilseed rape in the Huangshui basin were 216.59 km<sup>2</sup>, 782.34 km<sup>2</sup>, and 769.64 km<sup>2</sup>, accounting for 83.24%, 75.40%, and 71.35% of the planting area in 2002, respectively. The inflow areas of highland barley, spring wheat, and oilseed rape were 250.39 km<sup>2</sup>, 556.45 km<sup>2</sup>, and 648.23 km<sup>2</sup>, accounting for 85.17%, 68.55%, and 67.71% of the planting area in 2014, respectively. During this period, the outflow rates of highland barley, spring wheat, and oilseed rape in the Huangshui basin were 15.47 km<sup>2</sup>/year, 55.88 km<sup>2</sup>/year, and 54.97 km<sup>2</sup>/year, respectively, and the inflow rates were 20.87 km<sup>2</sup>/year, 46.37 km<sup>2</sup>/year, and 54.02 km<sup>2</sup>/year.

**Table 3.** Statistics on the transfer area of crops in the Huangshui basin from 2002 to 2022 (unit: km<sup>2</sup>).

		2002					Total Transfers in
		Highland Barley	Spring Wheat	Oilseed Rape	Other Crops	Other Land Types	
2014	Highland Barley		59.57	69.11	66.29	55.43	250.39
	Spring Wheat	38.64		244.08	229.17	44.57	556.45
	Oilseed Rape	62.97	212.83		291.12	81.32	648.23
	Other crops	51.15	277.70	281.53		364.47	974.86
	Other land types	63.83	232.24	174.93	830.26		1301.26
	Total transfers out	216.59	782.34	769.64	1416.84	545.79	
		2014					Total Transfers in
		Highland Barley	Spring Wheat	Oilseed Rape	Other Crops	Other land Types	
2022	Highland Barley		51.51	118.58	101.16	75.68	346.94
	Spring Wheat	27.98		177.14	179.64	82.40	467.17
	Oilseed Rape	56.72	242.88		160.09	58.65	518.34
	Other crops	66.48	160.77	232.31		347.20	806.76
	Other land types	62.83	106.46	154.54	756.11		1079.95
	Total transfers out	214.01	561.63	682.58	1197.00	563.93	
		2002					Total Transfers in
		Highland Barley	Spring Wheat	Oilseed Rape	Other Crops	Other Land types	
2022	Highland Barley		75.47	110.15	107.96	85.61	379.19
	Spring Wheat	27.02		193.84	247.78	59.93	528.58
	Oilseed Rape	47.35	198.50		220.16	70.14	536.15
	Other crops	47.73	229.74	241.49		307.50	826.46
	Other land types	90.35	345.23	276.32	1082.78		1794.67
	Total transfers out	212.46	848.93	821.79	1658.68	523.19	

From 2014 to 2022, the outflow areas of highland barley, spring wheat, and oilseed rape in the Huangshui basin were 214.01 km<sup>2</sup>, 561.63 km<sup>2</sup>, and 682.58 km<sup>2</sup>, accounting for 72.79%, 69.18%, and 71.30% of the planted areas in 2014, respectively. The inflow areas of highland barley, spring wheat, and oilseed rape were 346.94 km<sup>2</sup>, 467.17 km<sup>2</sup>, and 518.34 km<sup>2</sup>, accounting for 81.26%, 65.13%, and 65.36% of the planting areas in 2022, respectively. During the period from 2014 to 2022, the outflow rates of highland barley, spring wheat, and oilseed rape were 26.75 km<sup>2</sup>/year, 70.20 km<sup>2</sup>/year, and 85.32 km<sup>2</sup>/year, respectively, and the inflow rates were 43.37 km<sup>2</sup>/year, 58.40 km<sup>2</sup>/year, and 64.79 km<sup>2</sup>/year.

From 2002 to 2022, the increased area of highland barley mainly originated from the transfer of oilseed rape and other crops, accounting for 57.52% of the total area transferred to the highland barley. The decreased areas of spring wheat and oilseed rape were mainly converted to other crops and non-agricultural land, accounting for 67.72% and 63.01% of the total area transferred from spring wheat and oilseed rape, respectively.

### 3.4. Change Analysis of Crop Planting Structure Characteristics

From 2000 to 2022, the gravity center and the SDE of crop distribution in the Huangshui basin changed, as shown in Figure 6. The planting center of highland barley initially moved 22.61 km to the southeast, and then moved 16.95 km to the northwest. The planting center of spring wheat initially moved 4.67 km to the northwest, and then moved 7.73 km to the southeast. The planting center of oilseed rape initially moved northward by 2.83 km, and then moved northwestward by 5.95 km. The planting center of other crops initially moved eastward by 8.47 km and then westward by 4.73 km. During the study period, the overall trend of highland barley and spring wheat cultivation direction was towards the southeast,

and the cultivation direction of oilseed rape showed an overall northwest movement. The cultivation direction of other crops exhibited an overall eastward movement.

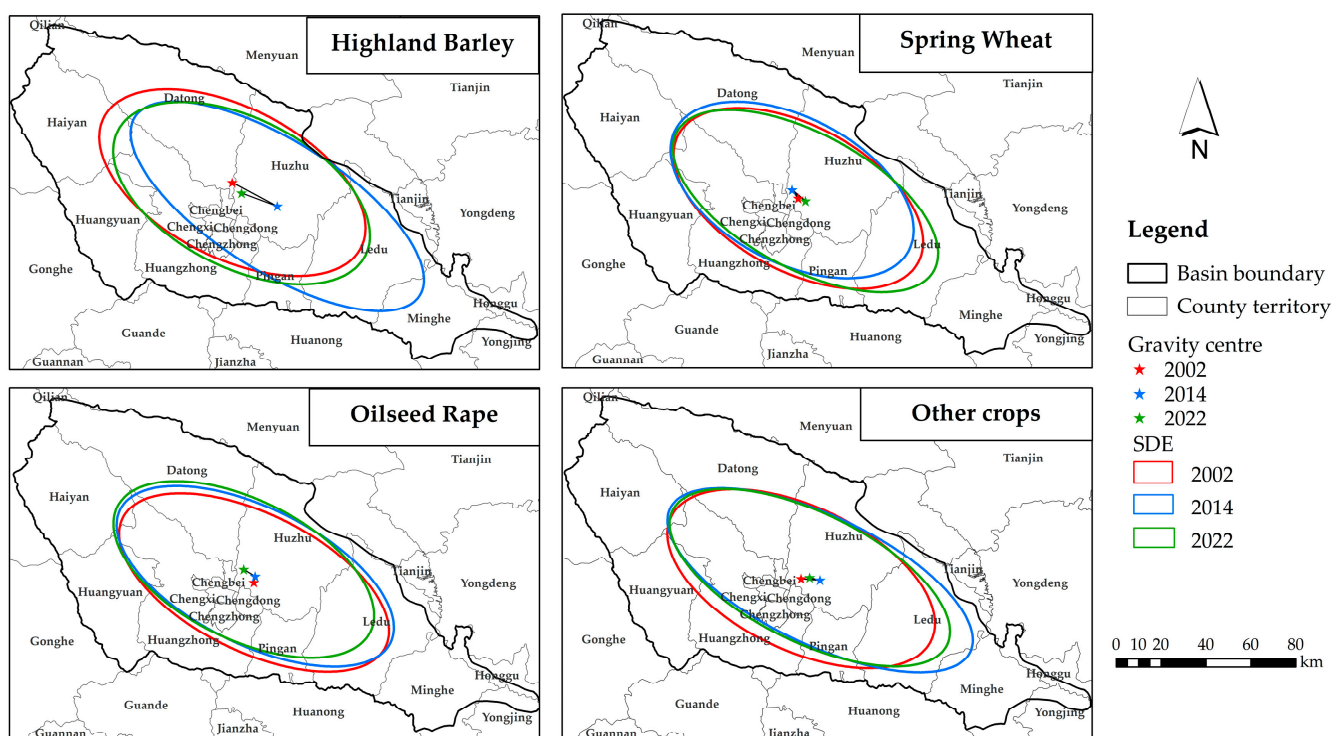


**Figure 6.** Gravity center and standard deviation ellipse of major crops in the Huangshui basin, including four categories of crops: highland barley, spring wheat, oilseed rape, and other crops in 2002, 2014, and 2022.

During the period from 2002 to 2014, the movement rates of the planting center for highland barley, spring wheat, oilseed rape, and other crops were 1.88 km/year, 0.39 km/year, 0.24 km/year, and 0.59 km/year, respectively. From 2014 to 2022, the movement rates of the gravity center for highland barley, spring wheat, oilseed rape, and other crops were 2.12 km/year, 0.97 km/year, 0.74 km/year, and 0.71 km/year, respectively.

The SDE of the major crops covered almost the entire central region of the Huangshui basin (Figure 6), exhibiting an overall northwest–southeast distribution. This region represents the core area of crop distribution in the Huangshui basin. Regarding the spatial distribution pattern (Table 4), the elliptic azimuth of highland barley cultivation shifted clockwise from 116.75° in 2002 to 122.02° in 2014, and then rotated counterclockwise to 116.63° in 2022. This indicates a shift in the region driven by highland barley cultivation, from the southeastern to the northwestern part of the Huangshui basin, while the opposite trend was observed for spring wheat. The elliptic azimuths of oilseed rape and other crop distributions continuously rotated clockwise, with the elliptic azimuth of oilseed rape changing from 116.07° in 2002 to 116.27° in 2022, and the elliptic azimuth of other crops changing from 115.30° in 2002 to 116.13° in 2022. This indicates that the southeastern part of the Huangshui basin serves as the driving region for oilseed rape and other crop cultivation.

Considering the central elevation of the SDE, the altitude of the highland barley and oilseed rape planting centers has shown an increasing trend, with an elevation of 183 m and 462 m, respectively. The altitude of the spring wheat planting center increased from 2002 to 2014, but decreased from 2014 to 2022. Overall, the altitude of the spring wheat planting center decreased by 242 m. The altitude of the other crops remained relatively stable from 2002 to 2014, but showed a decreasing trend from 2014 to 2022, with an overall decrease of 256 m.

**Table 4.** Standard deviation ellipsometric parameters for crops in the Huangshui basin in 2002, 2014, and 2022.

Crop	Year	Center Coordinate		X dist/km	Y dist/km	Rotation $\theta$ (°)	Elevation of Center (m)
		X/m	Y/m				
Highland Barley	2002	748,287	4,074,175	64.18	33.52	116.75	2365
	2014	768,298	4,063,647	74.86	29.04	122.02	2504
	2022	752,384	4,069,489	61.72	33.28	116.63	2548
Spring Wheat	2002	754,042	4,064,954	60.49	32.38	117.99	2522
	2014	751,269	4,068,716	58.52	32.39	117.26	2663
	2022	757,229	4,063,792	65.03	30.10	118.24	2280
Oilseed Rape	2002	756,783	4,061,854	65.18	30.71	116.07	2264
	2014	757,323	4,064,631	67.09	30.45	116.14	2289
	2022	752,215	4,067,687	62.86	31.04	116.27	2726
Other crops	2002	755,067	4,062,722	64.12	32.01	115.30	2564
	2014	763,514	4,062,034	74.07	28.59	115.53	2561
	2022	758,921	4,063,183	68.06	28.74	116.13	2305

## 4. Discussion

### 4.1. Impact of Data Sources, Feature Selection, and Classification Algorithms on Crop Extraction

Considering the temporal scope of this study, we opted for using freely available long time-series Landsat imagery as our foundational dataset. In the paper, we applied data fusion and vegetation-enhancement techniques to process the imagery, thereby improving its data quality. This data processing workflow can serve as a valuable reference for related research endeavors. However, without temporal constraints, the utilization of remote sensing data with higher temporal and spectral resolutions, such as the Sentinel's imagery, is expected to yield improved classification results.

To reduce the impact of mixed pixels, in addition to extracting traditional spectral features, this study also incorporated the NDVI, terrain, and texture features for crop classification. However, during the feature selection process, it was observed that the importance and retention of features varied across different years, indicating that the factors influencing crop classification are subject to changes in the environment. The initial selection of feature parameters in this study may have resulted in the omission of certain critical information. Therefore, there is room for further exploration and improvement in our approach. In future research, addressing the issues related to changing environmental conditions and feature importance across years will be crucial. Furthermore, incorporating environmental factors such as climate and precipitation into the classification process would be beneficial [53,54].

Comparing our results with existing research, Wang et al. [55] achieved the highest accuracy of 77.12% by comparing four machine learning models and two deep learning models combined with time-series satellite data for large-scale regional crop-type classification. Yan et al. [56], based on MODIS and Landsat imagery, constructed features using phenological parameters to extract crop information on the Qinghai–Tibet Plateau, with an overall accuracy of 86.23% and a kappa coefficient of 0.82. In this study, we employed a combination of feature selection and the ROF algorithm to classify crops in the Huangshui basin for 2002, 2014, and 2022, yielding an overall accuracy above 86.97% and a kappa coefficient above 0.824. The obtained crop classification accuracy in this paper exceeds that of the previous studies, indicating that the ROF algorithm, through the PCA's transformation of the selected feature subset, achieves better classification results. The method proposed in this paper provides a reference for implementing crop mapping in small- and medium-sized areas.

### 4.2. Spatial Evolution Characteristics of Crops

Regarding the analysis of crop transitions, it was found that the inflow of highland barley exceeded the outflow, resulting in an increase in the highland barley's cultivation

area. One possible reason for this is the rapid development of the liquor industry that relies on highland barley as a raw material, leading to a growing demand for highland barley. Another possible reason is the implementation of various subsidies by the government for highland barley cultivation, including breeding subsidies, promotion subsidies, and direct grain subsidies [38]. These policies have made highland barley cultivation more profitable compared to other crops, thereby promoting its cultivation in the basin. However, for oilseed rape and spring wheat, the outflow exceeded the inflow, leading to a decrease in cultivation area. One reason for this is the reduction in arable land, which has resulted in a decrease in the sowing area for major crops. Another reason is the shift in crop structure over the past 20 years, with a transition towards a diversified planting structure that includes oilseed rape, wheat, potatoes, and corn [57]. In the future planning of crop cultivation in this region, the government should not only promote the development of specialized agriculture but also strengthen farmland protection measures. It is essential to establish comprehensive farmland compensation policies to reduce instances of local farmers abandoning their fields, ensuring the preservation of arable land [58].

From 2002 to 2022, the gravity centers of crops in the Huangshui basin were mainly located in the central part, showing limited overall movement. The SDE exhibited a northwest–southeast trend, indicating a relatively stable dispersion pattern of crops. This is primarily attributed to the unique topography of the Huangshui basin, where the cultivation areas are predominantly located in the river-valley regions with relatively favorable natural environmental conditions [59]. However, due to the fragile ecological environment in this region, the following are true: the agricultural production capacity to withstand natural disasters is relatively low; soil fertility is declining year by year; and the area of high-quality arable land continues to shrink. The government can address these issues through land remediation efforts, enhancing local agricultural water infrastructure, and reducing land fragmentation in the shallow mountainous areas near river valleys to improve the quality of arable land.

In recent years, the intensification of global climate change has had a significant impact on agriculture in the Huangshui basin. During the period from 2002 to 2022, the center of the SDE for spring wheat and other crops shifted towards lower altitudes. On the other hand, the center of the SDE for highland barley and oilseed rape exhibited a migration towards higher altitudes. This finding is consistent with the findings of Ma's research [60] and can likely be attributed to the warming temperatures in the study area over the past two decades. Climate change is intensifying, with rising temperatures potentially affecting the seasonality of agricultural production and leading to shifts in crop planting boundaries [61]. Changes in precipitation patterns may lead to uneven rainfall, resulting in droughts or floods. These changes will present new challenges to agricultural development. The Ministry of Agriculture can adapt to these changes by establishing meteorological information and early-warning systems, introducing climate-adaptive crop varieties, improving water resource management, and implementing other measures to ensure the sustainability of local food production.

## 5. Conclusions

In crop extraction, the spectral, vegetation index, and terrain features have been found to be significantly more important than auxiliary features, such as texture, in this region. The performance of three classifiers—the SVM, RF, and ROF—was compared; the ROF algorithm achieved the best classification results. Based on the ROF algorithm, the overall accuracy of crop extraction was above 86.97%, and the kappa coefficient was above 0.824.

The spatial distribution of oilseed rape was the most widespread among the major crops grown in the Huangshui basin, followed by spring wheat, and then highland barley. The planting area of crops in the study area changed significantly from 2002 to 2022, and there was a noticeable shift in crop distribution.

During the study period, the SDE of crops was oriented in the northwest–southeast direction. Highland barley exhibited the highest degree of movement in its planting center,

followed by other crops, spring wheat, and Oilseed Rape. In the vertical direction, the planting centers of highland barley and oilseed rape migrated towards higher altitudes, while the planting centers of spring wheat and other crops showed a decreasing trend in altitude.

**Author Contributions:** Conceptualization, X.F. and W.Z.; methodology, X.F. and X.Z.; software, X.F.; validation, X.F. and W.Z.; formal analysis, X.F.; investigation, W.Z.; resources, W.Z.; data curation, X.F.; writing—original draft preparation, X.F.; writing—review and editing, X.F., W.Z. and Y.H.; visualization, X.F.; supervision, W.Z.; project administration, W.Z.; funding acquisition, W.Z. All authors have read and agreed to the published version of the manuscript.

**Funding:** This research received no external funding.

**Data Availability Statement:** Not applicable.

**Conflicts of Interest:** The authors declare no conflict of interest.

### Abbreviations

SVM	Support Vector Machine
RF	Random Forest
ROF	Rotation Forest
RF_RFE	Random Forest Recursive Feature Elimination
SDE	Standard Deviation Ellipse
KNN	K-nearest Neighbors
DT	Decision Tree
PCA	Principal Component Analysis
CLCD	China Land Cover Dataset
GEE	Google Earth Engine
GS	Gram-Schmidt Pan Sharpening
NDVI	Normalized Vegetation Index
DEM	Digital Elevation Model
NASA	United States' National Aeronautics and Space Administration
RBF	Radial Basis Function
UA	User Accuracy
PA	Producer Accuracy
AA	Average Accuracy
OA	Overall Accuracy
NIR	Near Infrared
SWIR	Short-wave Infrared
HB	Highland Barley
SW	Spring Wheat
OR	Oilseed Rape
OC	Other Crops

### References

1. Zhou, L.; Luo, J.; Fang, P. China's Food Security and Food Sovereignty in the 21st Century. *Chin. Rural Econ.* **2022**, *454*, 2–23.
2. Han, Y.; Meng, J. A review of per-field crop classification using remote sensing. *Remote Sens. Nat. Resour.* **2019**, *31*, 1–9.
3. Zhao, C. Advances of Research and Application in Remote Sensing for Agriculture. *Trans. Chin. Soc. Agric. Mach.* **2014**, *45*, 277–293.
4. Qiu, P.; Wang, X.; Cha, M.; Li, Y. Crop Identification Based on TWDTW Method and Time Series GF-1 WFV. *Sci. Agric. Sin.* **2019**, *52*, 2951–2961.
5. Chen, S.; Liu, Q.; Chen, L.; Li, J.; Liu, Q. Review of research advances in remote sensing monitoring of grain crop area. *Trans. Chin. Soc. Agric. Eng.* **2005**, *21*, 166–171.
6. Wang, Y.; Zhang, Z.; Zuo, L.; Wang, X.; Zhao, X.; Sun, F. Mapping Crop Distribution Patterns and Changes in China from 2000 to 2015 by Fusing Remote-Sensing, Statistics, and Knowledge-Based Crop Phenology. *Remote Sens.* **2022**, *14*, 1800. [[CrossRef](#)]
7. Segarra, J.; Buchailot, M.L.; Araus, J.L.; Kefauver, S.C. Remote Sensing for Precision Agriculture: Sentinel-2 Improved Features and Applications. *Agronomy* **2020**, *10*, 641. [[CrossRef](#)]

8. Sonobe, R.; Yamaya, Y.; Tani, H.; Wang, X.; Kobayashi, N.; Mochizuki, K.-i. Mapping crop cover using multi-temporal Landsat 8 OLI imagery. *Int. J. Remote Sens.* **2017**, *38*, 4348–4361. [[CrossRef](#)]
9. Zhang, H.; Li, Q.; Liu, J.; Du, X.; Dong, T.; McNairn, H.; Champagne, C.; Liu, M.; Shang, J. Object-based crop classification using multi-temporal SPOT-5 imagery and textural features with a Random Forest classifier. *Geocarto Int.* **2018**, *33*, 1017–1035. [[CrossRef](#)]
10. Sonobe, R.; Yamaya, Y.; Tani, H.; Wang, X.; Kobayashi, N.; Mochizuki, K.-i. Assessing the suitability of data from Sentinel-1A and 2A for crop classification. *GIScience Remote Sens.* **2017**, *54*, 918–938. [[CrossRef](#)]
11. Ren, T.; Xu, H.; Cai, X.; Yu, S.; Qi, J. Smallholder Crop Type Mapping and Rotation Monitoring in Mountainous Areas with Sentinel-1/2 Imagery. *Remote Sens.* **2022**, *14*, 566. [[CrossRef](#)]
12. Liang, J.; Zheng, Z.; Xia, S.; Zhang, X.; Tang, Y. Crop recognition and evaluation using red edge features of GF-6 satellite. *Natl. Remote Sens. Bull.* **2020**, *24*, 1168–1179. [[CrossRef](#)]
13. Chen, J.; Li, H.; Liu, Y.; Chang, Z.; Han, W.; Liu, S. Remote sensing recognition of agricultural crops based on Sentinel-2 data with multi-feature optimization. *Remote Sens. Nat. Resour.* **2023**, 1–9. Available online: <http://kns.cnki.net/kcms/detail/10.1759.P.20230531.0953.006.html> (accessed on 15 July 2023).
14. Lu, D.; Weng, Q. A survey of image classification methods and techniques for improving classification performance. *Int. J. Remote Sens.* **2007**, *28*, 823–870. [[CrossRef](#)]
15. Zhang, Y.; He, Z.; Wu, Z. Crop Classification and Extraction Based on Multi-Source Remote Sensing Image. *J. Shandong Agric. Univ.* **2021**, *52*, 615–618.
16. Fu, X.; Zhou, W.; Zhou, X.; Li, F.; Hu, Y. Classifying Mountain Vegetation Types Using Object-Oriented Machine Learning Methods Based on Different Feature Combinations. *Forests* **2023**, *14*, 1624. [[CrossRef](#)]
17. Guo, Y.; Yu, X.; Jiang, D.; Wang, S.; Jiang, X. Study on Forest Classification Based on Object Oriented Techniques. *J. Geo-Inf. Sci.* **2012**, *14*, 514–522. [[CrossRef](#)]
18. Chen, Y.; Mo, W.; Mo, J.; Wang, J.; Zhong, S. Object-oriented Classification for the Extraction of Rice Planting Area in South. *Remote Sens. Technol. Appl.* **2011**, *26*, 163–168.
19. Luo, C.; Qi, B.; Liu, H.; Guo, D.; Lu, L.; Fu, Q.; Shao, Y. Using Time Series Sentinel-1 Images for Object-Oriented Crop Classification in Google Earth Engine. *Remote Sens.* **2021**, *13*, 561. [[CrossRef](#)]
20. Tian, Y.; Yang, C.; Huang, W.; Tang, J.; Li, X.; Zhang, Q. Machine learning-based crop recognition from aerial remote sensing imagery. *Front. Earth Sci.* **2021**, *15*, 54–69. [[CrossRef](#)]
21. Zhang, J.; Feng, L.; Yao, F. Improved maize cultivated area estimation over a large scale combining MODIS–EVI time series data and crop phenological information. *ISPRS J. Photogramm. Remote Sens.* **2014**, *94*, 102–113. [[CrossRef](#)]
22. Kang, J. Research on Extraction Method of Crop Planting Structure Based on Machine. Master’s Thesis, Wuhan University, Wuhan, China, 2020.
23. Saleem, M.H.; Potgieter, J.; Arif, K.M. Automation in Agriculture by Machine and Deep Learning Techniques: A Review of Recent Developments. *Precis. Agric.* **2021**, *22*, 2053–2091. [[CrossRef](#)]
24. Huang, S.; Yang, L.; Chen, X.; Yao, Y. Study of Typical Arid Crops Classification Based on Machine Learning. *Spectrosc. Spectr. Anal.* **2018**, *38*, 3169–3176.
25. Erdanaev, E.; Kappas, M.; Wyss, D. Irrigated Crop Types Mapping in Tashkent Province of Uzbekistan with Remote Sensing-Based Classification Methods. *Sensors* **2022**, *22*, 5683. [[CrossRef](#)] [[PubMed](#)]
26. Fang, P.; Zhang, X.; Wei, P.; Wang, Y.; Zhang, H.; Liu, F.; Zhao, J. The Classification Performance and Mechanism of Machine Learning Algorithms in Winter Wheat Mapping Using Sentinel-2 10 m Resolution Imagery. *Appl. Sci.* **2020**, *10*, 5075. [[CrossRef](#)]
27. Chen, G.; Xie, X.; Li, S. Research on Complex Classification Algorithm of Breast Cancer Chip Based on SVM-RFE Gene Feature Screening. *Complexity* **2020**, *2020*, 1342874. [[CrossRef](#)]
28. Cheng, K.; Wang, J. Forest Type Classification Based on Integrated Spectral-Spatial-Temporal Features and Random Forest Algorithm—A Case Study in the Qinling Mountains. *Forests* **2019**, *10*, 559. [[CrossRef](#)]
29. Breiman, L. Random Forests. *Mach. Learn.* **2001**, *45*, 5–32. [[CrossRef](#)]
30. Rodriguez, J.J.; Kuncheva, L.I. Rotation forest: A new classifier ensemble method. *IEEE Trans. Pattern Anal. Mach. Intell.* **2006**, *28*, 1619–1630. [[CrossRef](#)]
31. Peng, L.; Liu, K.; Zhu, Y.; Liu, L. GF-2 Satellite Imagery Application in Land Use Classification Based on Rotation Forest Algorithm. *Spacecr. Recovery Remote Sens.* **2019**, *40*, 112–122.
32. Zhou, E.; Gao, S. A Cost-Sensitive Rotating Forest Classification Algorithm. *Comput. Digit. Eng.* **2021**, *49*, 1763–1766+1883.
33. Fu, X.; Zhou, W.; Zhou, X.; Li, F. Application of Machine Learning in Vegetation Interpretation of Natural Protected Areas in Jiuzhaigou County. *Nat. Prot. Areas* **2023**, *3*, 53–65. [[CrossRef](#)]
34. Song, Q.; Hu, Q.; Lu, M.; Yu, Q.; Yan, P.; Shi, Y.; Duan, Y.; Wu, W. Prospect of crop mapping. *Chin. J. Agric. Resour. Reg. Plan.* **2020**, *41*, 57–65.
35. Wei, H.; Lu, C.; Liu, Y. Farmland Changes and Their Ecological Impact in the Huangshui River Basin. *Land* **2021**, *10*, 1082. [[CrossRef](#)]
36. Wang, R.; Bai, D.; Yin, F. Trends and Continuity Analysis of Vegetation Change in Huangshui River Basin from 2000 to 2019. *Remote Sens. Technol. Appl.* **2022**, *37*, 1504–1512.

37. Yuan, Y. Farmland Water Conservancy Rural Economy The Republic Of China in Qinghai. *J. Qinghai Minzu Univ. (Soc. Sci.)* **2019**, *45*, 118–127.
38. Tian, L. The Extraction of crop Planting Structure and Its Dynamic Monitoring of Huangshui Basin from 2000 to 2015 Combined with STARFM Model. Master's Thesis, Southwest University, Chongqing, China, 2018.
39. Yang, J.; Huang, X. The 30 m annual land cover dataset and its dynamics in China from 1990 to 2019. *Earth Syst. Sci. Data* **2021**, *13*, 3907–3925. [[CrossRef](#)]
40. Zang, Y.; Qiu, Y.; Chen, X.; Chen, J.; Yang, W.; Liu, Y.; Peng, L.; Shen, M.; Cao, X. Mapping rapeseed in China during 2017–2021 using Sentinel data: An automated approach integrating rule-based sample generation and a one-class classifier (RSG-OC). *GIScience Remote Sens.* **2023**, *60*, 2163576. [[CrossRef](#)]
41. Cheng, M. Long time series (2001–2015) high-resolution crop yield and water productivity dataset of China. *Zenodo* **2021**. [[CrossRef](#)]
42. Shen, Y.; Zhang, J.; Yang, L.; Zhou, X.; Li, H.; Zhou, X. A Novel Operational Rice Mapping Method Based on Multi-Source Satellite Images and Object-Oriented Classification. *Agronomy* **2022**, *12*, 3010. [[CrossRef](#)]
43. Song, Q. Crop mapping and spatio-temporal analysis of agricultural Land-use. Ph.D. Thesis, Chinese Academy of Agricultural Sciences, Beijing, China, 2018.
44. Yang, S.; Gu, L.; Li, X.; Jiang, T.; Ren, R. Crop Classification Method Based on Optimal Feature Selection and Hybrid CNN-RF Networks for Multi-Temporal Remote Sensing Imagery. *Remote Sens.* **2020**, *12*, 3119. [[CrossRef](#)]
45. Cortes, C.; Vapnik, V. Support-vector networks. *Mach. Learn.* **1995**, *20*, 273–297. [[CrossRef](#)]
46. Son, N.-T.; Chen, C.-F.; Chen, C.-R.; Minh, V.-Q. Assessment of Sentinel-1A data for rice crop classification using random forests and support vector machines. *Geocarto Int.* **2018**, *33*, 587–601. [[CrossRef](#)]
47. Bao, J.; Yu, L.; Wulan, T.; Xu, H.; Wuyun, D.; Yu, W. Research on crop remote sensing recognition method based on a random forest method—Take some areas of Arun Banner as an example. *Agric. Henan* **2020**, *558*, 62–64. [[CrossRef](#)]
48. Lu, H.; Meng, Y.; Yan, K.; Gao, Z. Kernel principal component analysis combining rotation forest method for linearly inseparable data. *Cogn. Syst. Res.* **2019**, *53*, 111–122. [[CrossRef](#)]
49. Yang, X.; Guo, B.; Lu, Y.; Zhang, R.; Zhang, D.; Zhen, X.; Chen, S.; Wu, H.; Wei, C.; Yang, L.; et al. Spatial-temporal evolution patterns of soil erosion in the Yellow River Basin from 1990 to 2015: Impacts of natural factors and land use change. *Geomat. Nat. Hazards Risk* **2021**, *12*, 103–122. [[CrossRef](#)]
50. Guo, W. Distribution and Spatial-Temporal Variation of Winter Wheat Based on Integrating of Remote Sensing and Statistical Data. Master's Thesis, Chinese Academy of Agricultural Sciences, Beijing, China, 2018.
51. Yuill, R.S. The Standard Deviation Ellipse; An Updated Tool for Spatial Description. *Geogr. Ann. Ser. B Hum. Geogr.* **1971**, *53*, 28–39. [[CrossRef](#)]
52. Guo, R.; Zhu, X.; Zhang, C.; Cheng, C. Analysis of Change in Maize Plantation Distribution and Its Driving Factors in Heilongjiang Province, China. *Remote Sens.* **2022**, *14*, 3590. [[CrossRef](#)]
53. Bichler, B.; Lippert, C.; Haring, A.M.; Dabbert, S. The determinants of the spatial distribution of organic farming in Germany. *Berichte Uber Landwirtschaft* **2005**, *83*, 50–75.
54. Liu, Y.; Zhou, Q.; Lu, Y.; Li, H. Agricultural Climate Resource Change of Huang Shuihe Region in Recent 50 Years. *Chin. Agric. Sci. Bull.* **2016**, *32*, 163–170.
55. Wang, X.; Zhang, J.; Xun, L.; Wang, J.; Wu, Z.; Hanchiri, M.; Zhang, S.; Zhang, S.; Bai, Y.; Yang, S.; et al. Evaluating the Effectiveness of Machine Learning and Deep Learning Models Combined Time-Series Satellite Data for Multiple Crop Types Classification over a Large-Scale Region. *Remote Sens.* **2022**, *14*, 2341. [[CrossRef](#)]
56. Yan, J.; Zhang, M.; Zhang, S. Information Extraction of Main Crops in Eastern Qinghai Province Based on GEE Platform and MODIS NDVI Time Series. *J. Southwest Univ.* **2023**, *45*, 55–64. [[CrossRef](#)]
57. Chen, Y.; Zhou, Q.; CHEN, Q.; Mao, X.; Liu, F. The response of grain crops in Hehuang Valley to the climate change nearly 20 years. *Agric. Res. Arid Areas* **2018**, *36*, 223–229+241.
58. Yanyan, L.; Chen, Q.; Liu, F.; Zhou, Q.; Xu, H.; Ma, W. Analysis on the influencing factors of farmland abandoning behaviors in the northeastern Qinghai-Tibet Plateau: A case study of the upper reaches of Huangshui River. *Res. Agric. Mod.* **2019**, *40*, 993–1001. [[CrossRef](#)]
59. Luo, J.; Chen, Q.; Liu, F.; Zhang, Y.; Zhou, Q. Methods for reconstructing historical cropland spatial distribution of the Yellow River–Huangshui River valley in Tibetan Plateau. *Prog. Geogr.* **2015**, *34*, 207–216.
60. Ma, W. Evaluation of Impact of Climate Change on Highland Barley Cultivation in Qinghai-Tibet Plateau. Ph.D. Thesis, Qinghai Normal University, Xining, China, 2022.
61. Yang, X.; Chen, F.; Lin, X.; Liu, Z.; Zhang, H.; Zhao, J.; Li, K.; Ye, Q.; Li, Y.; Lv, S.; et al. Potential benefits of climate change for crop productivity in China. *Agric. For. Meteorol.* **2015**, *208*, 76–84. [[CrossRef](#)]

**Disclaimer/Publisher's Note:** The statements, opinions and data contained in all publications are solely those of the individual author(s) and contributor(s) and not of MDPI and/or the editor(s). MDPI and/or the editor(s) disclaim responsibility for any injury to people or property resulting from any ideas, methods, instructions or products referred to in the content.